Comput Geosci (2013) 17:1015–1031
DOI 10.1007/s10596-013-9372-0

ORIGINAL PAPER

Training image-based scenario modeling of fractured reservoirs for flow uncertainty quantification

Andre Jung · Darryl H. Fenwick · Jef Caers

Received: 1 April 2013 / Accepted: 21 August 2013 / Published online: 10 September 2013

Abstract Geological characterization of naturally fractured reservoirs is potentially associated with large uncertainty. However, the geological modeling of discrete fracture networks (DFN) is considerably disconnected from uncertainty modeling based on conventional flow simulators in practice. DFN models provide a geologically consistent way of modeling fractures in reservoirs. However, flow simulation of DFN models is currently infeasible at the field scale. To translate DFN models to dual media descriptions efficiently and rapidly, we propose a geostatistical approach based on patterns. We will use experimental design to capture the uncertainties in the fracture description and generate DFN models. The DFN models are then upscaled to equivalent continuum models. Patterns obtained from the upscaled DFN models are reduced to a manageable set and used as training images for multiple-point statistics (MPS). Once the training images are obtained, they allow for fast realization of dual-porosity descriptions with MPS directly, while circumventing the time-consuming process of DFN modeling and upscaling. We demonstrate our ideas on a realistic Middle East-type fractured reservoir system.

Keywords Fracture modeling · Discrete fracture networks · Geostatistics · Pattern modeling · Dual medium · Uncertainty quantification

A. Jung (✉) · J. Caers
Department of Energy Resources Engineering,
Stanford University, Stanford, CA 94305, USA
e-mail: ajung@stanford.edu

D. H. Fenwick
Streamsim Technologies, San Francisco, CA 94121, USA

1 Introduction

Realistic description of uncertainty and predictive power of reservoir models is dependent upon the ability to model geological phenomena. This is especially true for naturally fractured reservoirs (NFR), which can bear risks such as early water breakthrough and poor oil recovery. However, the evaluation and modeling of NFRs often bear shortcomings. In common modeling practice, two kinds of models for NFRs are employed: highly detailed, geologically realistic models built by geologists, and coarse, grid-based models used by engineers for reservoir flow simulations following the dual media paradigm [1–3]. The former are complicated, complex, and time-consuming discrete fracture network models (DFN); the latter are geo-cellular, i.e., grid-based models for use with conventional flow simulators in many cases partly or entirely disconnected from the underlying geology.

Building one geologically realistic DFN model for a fractured reservoir can be tedious and time-consuming. Building hundreds or even thousands of DFN models and running flow simulation at reservoir scale for the purpose of sensitivity analysis and uncertainty quantification of reservoir production is infeasible for practitioners. Simulating flow with conventional flow simulators which requires the upscaling of the flow properties of each DFN model to effective dual media properties on a grid is again a time-consuming process. Therefore, limiting the DFN modeling and upscaling, and instead directly modeling the effective properties in a geologically consistent manner would be advantageous. However, natural fractures comprise a complex system [4] and their characterization in the reservoir is associated with many uncertain-

ties (e.g., [5]) which must be captured in the dual media model.

We propose a methodology based on multiple-point statistics (MPS) for fast and geologically consistent generation of dual media models for the purpose of uncertainty modeling in NFRs. MPS represents a group of geostatistical algorithms for stochastic pattern reproduction ([6–8]; an overview is provided in [9, 10]). MPS borrows the patterns to be reproduced from so-called training images and has been successfully applied to simulate depositional structures of rocks (facies and petrophysical properties). The bottleneck for applying MPS wide-scale is the training image. We describe a methodology to obtain a manageable set of training images for the fractured medium of dual medium models. Creating such a set achieves two goals: firstly, rapid dual medium generation via MPS while maintaining geological realism, and secondly, realistic dual medium scenarios and therefore realistic uncertainty. In structural modeling [11, 12] as well as facies modeling [13–16], such (discrete) scenario-type uncertainty has proven to be one of the critical sources of geological uncertainty.

To obtain the set of training images, an extensive set of DFNs representing potential geological scenarios is generated and upscaled to effective properties. For each model, we also generate a binary map of the flow model. This binary map is derived from the key observation that in the reservoir flow model, not all grid blocks must have two media—only the grid blocks which contain a connected fracture network should be described in this manner [17]. The pattern in this map is based on fracture intensity per grid cell and determines which grid cells should be represented by a dual medium (connected fractures and matrix) or a single medium (disconnected fractures and matrix) in the flow simulation. These patterns are clustered based on their pattern-based distances to identify representative models to serve as training images. The training images are then employed to generate directly flow models with MPS.

We would like to address three common misunderstandings upfront. First, we do not construct training images for DFN models; instead, we work with effective properties in the grid domain. Second, we do not discretize fractures on the grid; instead, we deal with a large number of fractures per grid cell. We also do not simulate large-scale fractures or fracture corridors by means of MPS (e.g., [18]). Third, the aim of this workflow is not to build a small number of highly accurate fracture models; instead, we are interested in evaluating realistic uncertainty of the reservoir flow response which requires constructing a large number of flow models.

2 Methodology

2.1 Overview

First we will outline broadly the methodology and then use an example to illustrate the details of this workflow. Our workflow consists of various components that already exist in the literature; hence, the novelty lies in integrating them into a practical workflow applicable to real field applications. This also means that various components (such as upscaling) can be exchanged based on one's own personal experience.

Step 1: This step consists of the usual geological work relating to understanding and describing the fractured system. The goal here is to specify the various concepts as well as input parameters related to fractured modeling.

Step 2: Generation of DFN scenarios based on the data gathered in step 1. Experimental design can be used to limit the amount of scenarios generated.

Step 3: Translation of the DFN models to dual medium scenarios consisting of modeling an indicator for dual and single medium cells. This step upscales the DFN models to effective properties for dual medium. From this step on, we no longer deal with DFNs. The translation of the upscaled scenarios into a set of dual medium scenarios is represented through patterns.

Step 4: Selection of a set of representative dual medium scenarios by means of distance-based clustering. This scenario selection is based purely on the patterns found on the upscaled models; no flow simulation is applied at this point.

Step 5: Use the representative scenarios as training images for MPS to generate nonstationary geostatistical realizations of effective properties ready for flow simulation.

Step 6: Run flow simulation to assess uncertainty of a desired flow response.

2.2 Case study description

To demonstrate and illustrate our methodology, we have constructed a model analogous to fractured reservoirs in the Middle East (e.g., [19]). In this synthetic but realistic model, we aim to represent various elements common to fractured reservoirs such as uncertainty in interpretation or presence of seismic data.

The dominating structure in our case is a North–South striking anticline which is accompanied by buckle folds to both sides (Fig. 1a). The model extends 18.6 km in X (East–West) and 15.7 km in Y (North–South) direction represented by 102 × 86 grid cells with a horizontal dimension of 600 × 600 ft. The model has one layer with a thickness of 25 ft. The initial oil–water contact is at 6,100 ft. The reservoir is produced with 45 wells, of which 18 are water injections wells and 27 are production wells. There is also pressure support from the aquifer. The position of the wells is shown in Fig. 1a. Injectors are marked blue and producers are red. The water injection takes place at a constant bottom hole pressure of 4,000 psi with a maximum allowable rate of 5,000 stb/day. The total liquid production rate at each well is set to 2,000 stb/day. Throughout the production time of 3,000 days, the oil pressure stays above

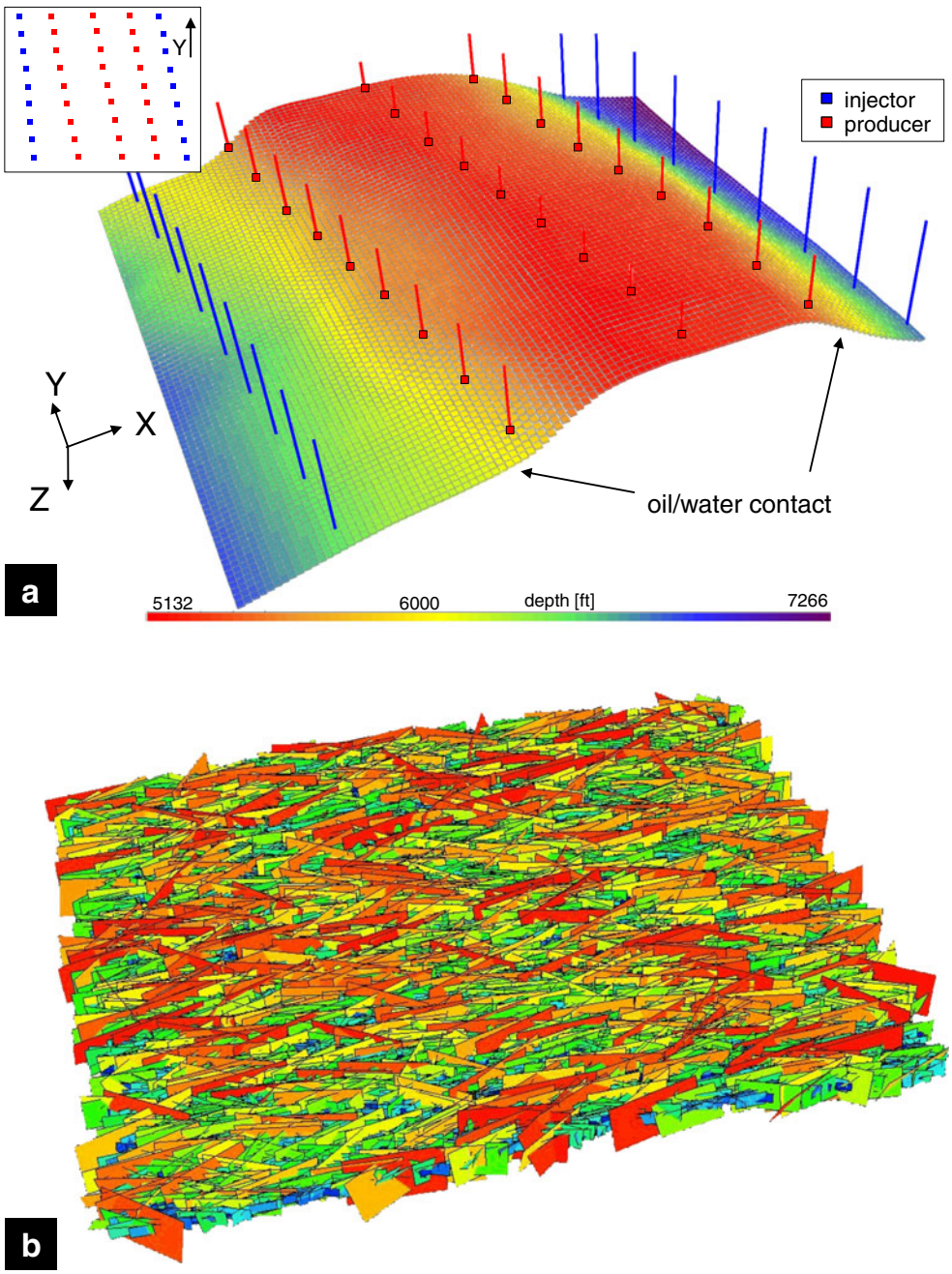

Fig. 1 **a** The reservoir model extends 18.6 km in X (East–West) and 15.7 km in Y (North–South) directions and comprises a North–South striking anticline. The 18 injectors are placed to both sides of the anticline, and the 27 producers are located around the hinge. The grid consists of 102 × 86 × 1 cells with cell dimensions of 600 × 600 × 25 ft. **b** A complex DFN model for the reservoir consisting of approximately 12,000 individual fractures

bubble point (no free gas). We employed a streamline simulator using the dual-porosity, single-permeability model to calculate the flow responses [20]. We are interesting in the surface oil production rate and cumulative oil production. Note that since there is no free gas, and we are imposing total rate at the producers, the sum of the oil and water rate is constant.

The permeability and porosity of the rock matrix is not the focus of this modeling approach and is kept constant at 200 mD and 20 %—typical values for carbonate reservoirs in the Middle East [21]. From here on, the term "effective properties" refers to the effective properties of the fractured medium in a dual medium approach (Fig. 2), specifically the fracture porosity ($\emptyset_f$), the fracture permeabilities (k_{fx}, k_{fy}, k_{fz}), and the shape factor sigma (σ). The sigma shape factor describes the fracture/matrix exchange [22].

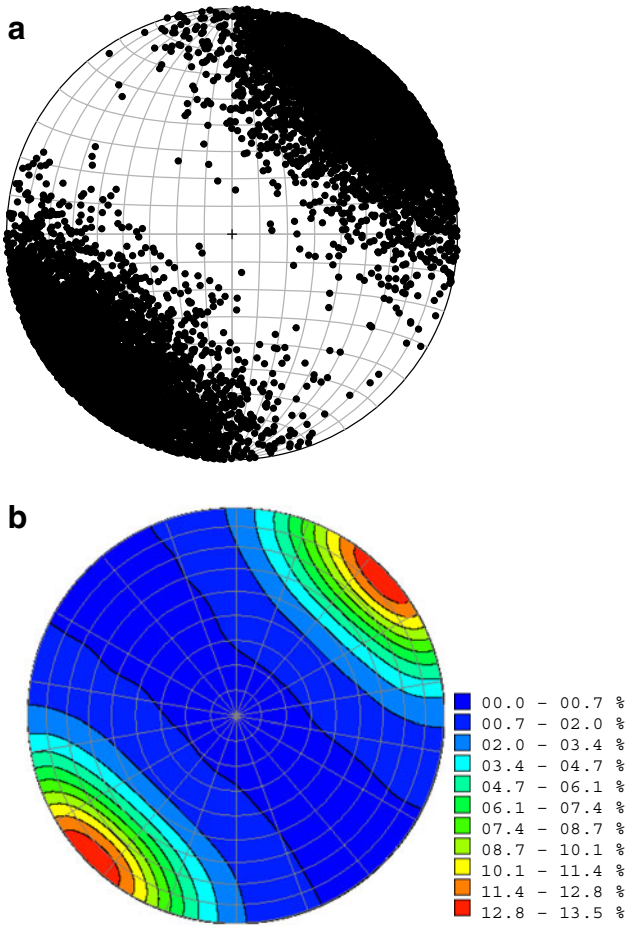

Fig. 2 Orientation distribution of one realization of one fracture set consisting of 12,167 individual fractures. The trend of the pole vectors to the fractures was set to 45° during fracture generation. The spread of the poles is determined by the dispersion factor of the Fisher orientation distribution (8 in this example). **a** Schmidt net with equal area projection of the poles in the lower hemisphere, generated using RFOC [42–47]. **b** Contoured density of the poles, generated using Fracman

In our case study, as well as in real reservoirs, multiple geological scenarios of the fracture system arise from the interpretation of data such as well-log, borehole imaging, seismic and /or outcrop data. The hinges of folds—here the anticline structure—tend to have higher intensity of fractures (e.g., [23, 24]). Although the analysis of the curvature can be used as an indicator for fracture intensity (e.g., [25]), orientation of fractures are difficult to predict (e.g., [26]). A seismic coherence attribute may indicate the presence of fracture networks. A low coherence typically corresponds to a higher intensity of fractures (e.g., [27, 28]). The formation of fracture corridors is a common feature of fractured reservoirs (e.g., [29, 30]). In our case, we mimic corridors of high fracture intensity as it can be derived from seismic coherence (Fig. 7a). We now implement the various details of our methodology within the context of this case.

2.3 Generating the DFN models (step 1 and 2)

To obtain DFN models reflecting the potential scenarios, we designed a full factorial design experiment on conceptual as well as parameter uncertainties (although the modeler may opt for a full Monte Carlo should this be feasible). The conceptual uncertainty comprises the spatial distribution of fracture intensity and the presence (or absence) of different fracture sets. The curvature of the anticline and corridors of decreased seismic coherence are assumed to be indicators for variations in the fracture intensity. Fracture intensity can also be regarded as an indirect measure of fracture intersections and is expressed as the P_{32} describing fracture area per volume [31]. For our models, we have set the average target intensity to 0.06. Variations in the length, trend, and orientation distribution of the fractures are considered as parameter uncertainties. Fracture parameters such as length and orientation are sampled from power law and Fisher distributions, respectively, during the stochastic generation of a DFN [32, 33]. Large-scale fractures, i.e., faults, providing long-distance connectivity (or barriers) are not modeled here. In the scope of this study, we considered the hydraulic parameters of the explicit fractures permeability, aperture, and compressibility as constant with the values 10D, 300 μm, and 10^{-5}kPa^{-1}, respectively. In reality, these values may vary due to the differences in length and roughness of individual fractures [34–36]. The dispersion or concentration factor, respectively, of 8 for the Fisher orientation distribution provides a large degree of freedom in the three-dimensional fracture orientation allowing fractures from one set to intersect (Fig. 2). The experimental design shown in Table 1 led to 156 ($2^4 \times 3^2 + 2^2 \times 3$) DFN models. To account for the spatial uncertainty of the DFN, we have generated four realizations for each scenario leading to a total of 624 models. One DFN realization is shown in Fig. 1b.

Table 1 Parameter variations used for the experimental design leading to 156 combinations; shown here, the scenarios of the fracture network

Presence of second fracture set	Yes	No	
Fracture set 1: size (powerlaw distribution of equiv. radius with D = 2, trunc. at 3,000 ft, aspect ratio 2:1)	400 ft	600 ft	
Fracture set 2: size (powerlaw distribution of equiv. radius with D = 2, trunc. at 3,000 ft, aspect ratio 2:1)	200 ft	400 ft	
Fracture set 1: trend of pole vectors (orientation distribution: Fisher with dispersion = 8)	0°	45°	
Fracture set 2: trend of pole vectors (orientation distribution: Fisher with dispersion = 8)	30°	60°	
Fracture set 1: intensity correlated with folding (curvature)	No	Weak	Strong
Fracture set 2: intensity correlated with fracture corridor (seismic coherence)	No	Weak	Strong

2.4 Translating DFN models to dual medium models and effective properties (step 3)

In this step, we translate the discrete fracture networks to a dual medium reservoir models by determining which grid cells are single medium (matrix only) and which cells qualify for dual medium. We then populate the fractured medium of the dual medium cells with effective properties (Fig. 3). Each DFN is represented by a dual medium model for use with conventional flow simulators. The methods described in this section are standard approaches and do not constitute the main contribution of this paper. In the scope of this study, we did not consider large fractures with long-range connectivity. In the presented test case, the fracture intensity is varying between grid cells. Grid cells without sufficient fracture connectivity are simulated as single medium, i.e., only the properties of the matrix are considered. To control which cells are simulated as dual medium,

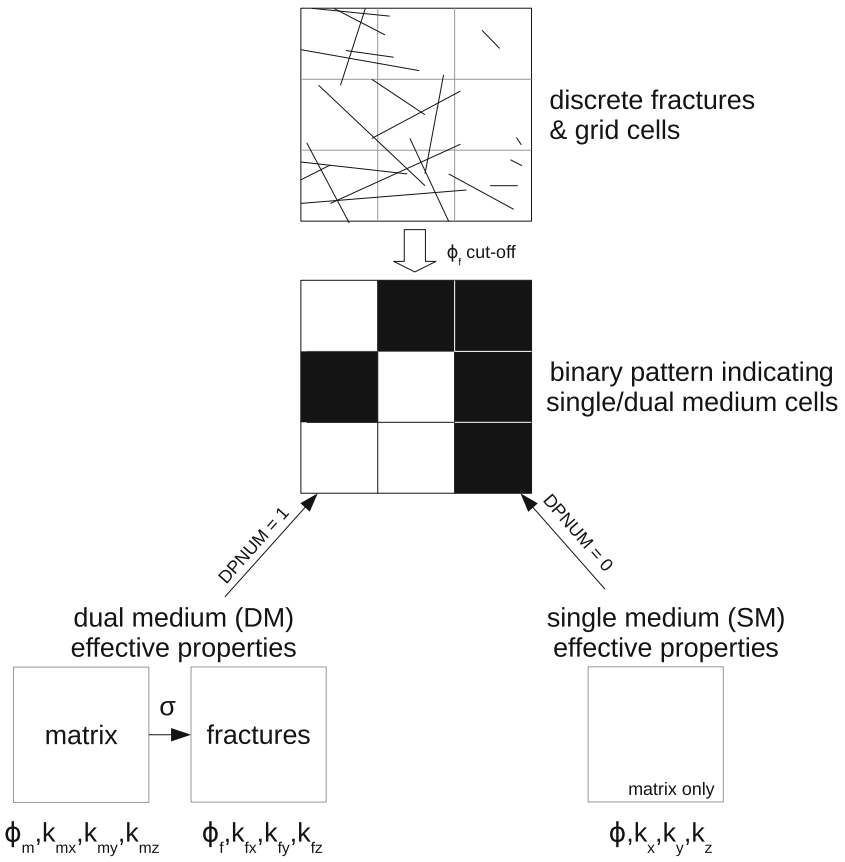

Fig. 3 Only grid cells with sufficient fracture connectivity are simulated as dual medium, for the case study here in single-permeability/dual-porosity mode. The remaining cells are simulated as single medium, i.e., only the matrix (nonfractured medium) is considered. In reservoirs with varying fracture intensity not all cells are equally fractured and consequently not all cells are modeled as dual medium. The detection of dual medium cells is based on a cutoff applied to fracture porosity. Dual medium cells are in *white*, single medium cells are *black*. The resulting binary pattern reflects the spatial variability of fracture intensity and connectivity, respectively. To demonstrate the robustness of the method, we increase and decrease the threshold by 10 % which in turn switches in average 10 % of the grid cells (approx. 850 cells) from single to dual medium and vice versa (discussed in detail in the Section 3)

we employed an auxiliary binary property "DPNUM". Cells with a DPNUM value of 1 are simulated as dual medium, cell with DPNUM equal to 0 are run single medium. For single medium cells, only the matrix properties are available. Various approaches exist to detect which cells need to be considered as dual medium. We have decided to determine dual medium cells based on a cutoff value of the fracture porosity, which is highly correlated with the fracture intensity. The fracture porosity can be calculated rapidly based on the volume of fractures present in one grid cell: $\emptyset_f = P_{32}$ * aperture. The histogram of the fracture porosity of one flow model and cutoff is shown in Fig. 4. Based on this histogram, for our experiment, we consider all cells with fracture porosity greater than 10^{-5} to contain dual media. Cells with fracture porosity less than the cutoff are considered to have disconnected fractures and thus should not be modeled using the dual medium paradigm. In reality, cells with the same fracture porosity or intensity, respectively, do not necessarily show the same connectivity. A probability function associated with the cutoff could potentially lead to a more realistic identification of dual medium cells. A constant cutoff appears to be a reasonable choice because even a variation of the threshold of 10 % did not affect the uncertainty quantification as discussed in Section 3 of this paper. Figure 5 shows one flow model with dual media cells (white) and single media (black). The binary pattern reflects the underlying connected fracture network as determined by the DFN model and porosity cutoff. As discussed in Section 3 of this paper, the binary pattern, i.e., spatial arrangement, of dual media cells governs the flow response. For the effective properties, the fracture porosity and sigma factor can be obtained directly. However, the upscaling of the fracture permeability is not trivial and can be done

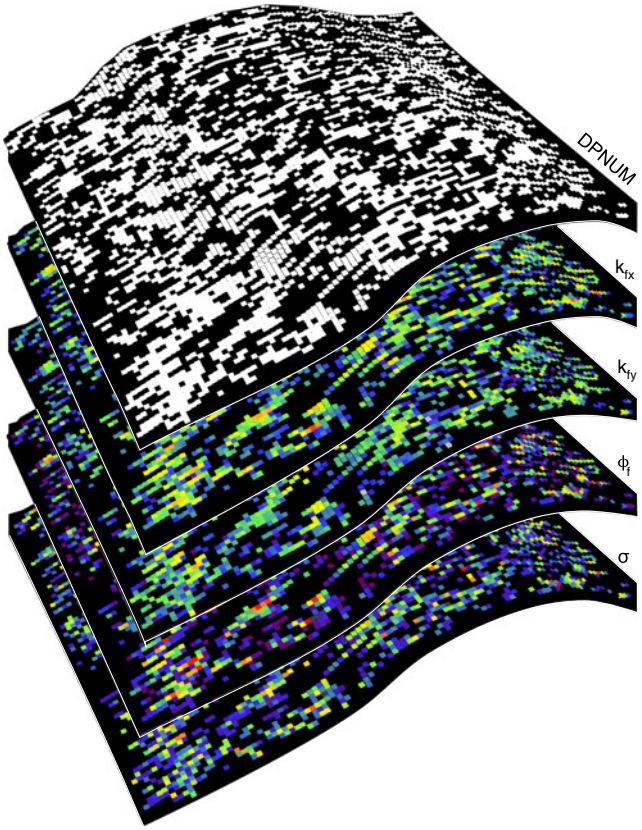

Fig. 5 A reservoir model of the effective properties of the fractured medium and sigma. The properties are only considered for dual medium cells. The white cells of the binary DPNUM pattern map are in dual medium mode (DPNUM = 1), the *black* cells are treated as single medium (DPNUM = 0). The binary map acts as a stencil for the effective properties

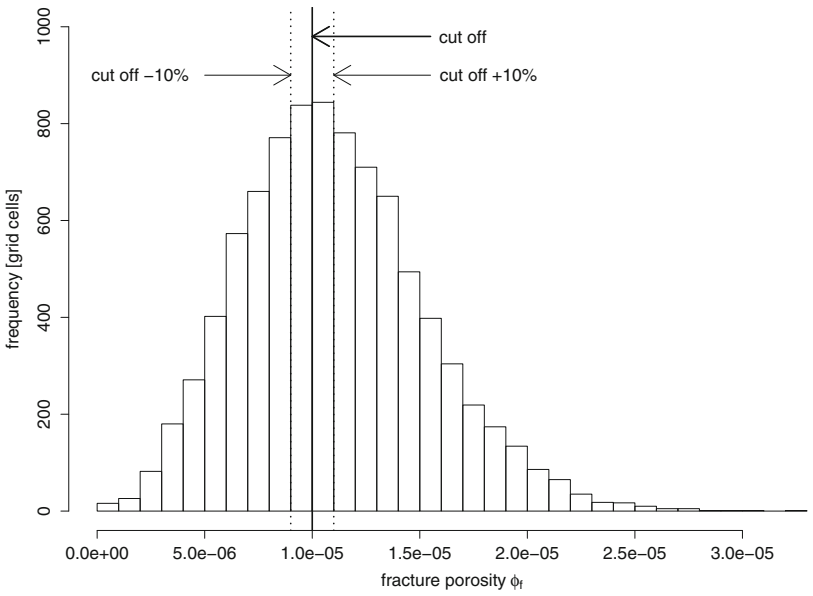

Fig. 4 Histogram of the fracture porosity of all 8,772 grid cells of one model. Grid cells with fracture porosity above the cutoff at 10^{-5} are handled as dual medium cells, the rest as single medium. The histogram shows also the increase and decrease of the cutoff value by 10 % as used for the sensitivity study on the patterns in the Section 3 of the paper (see Figs. 12, 13, 14, and 15). Notice that for this model, increasing the cutoff by 10 % switches 838 cells from dual to single medium. In the same way, decreasing the threshold by 10 % transforms 844 cells from single to dual medium

analytically or flow based. We have opted for the analytical method of Oda [37] as it is substantially faster than flow-based upscaling. Although Oda is not accurate for grid cells with low fracture intensity, it provides reasonable approximations, and its speed makes it the method of choice for practitioners. The workflow however allows for any upscaling technique to be employed. We use a diagonal tensor representation for fracture permeability as this is what is currently feasible in commercial simulators.

2.5 Obtaining a representative set of training images (step 4)

Due to the complexity of fracture modeling (and its large uncertainty), one may not be able to identify easily impacting input parameters that affect flow. Yet, in real cases, reservoir engineers can rarely handle hundreds of fracture models or scenarios. Therefore, we propose to reduce the set of all 156 possible scenarios to a more manageable set. We propose not to work on parameter reduction but on pattern reduction [38]. At the same time, this reduced set needs to cover a similar uncertainty in flow as the original set. This will be demonstrated later on in this paper.

To reduce the set of patterns yet maintain pattern diversity, we employ a distance-based selection approach [15, 16, 38, 39]. The methodology presented in those papers was applied to facies models (categorical variables), and due to the translation of DFN to dual medium patterns, now becomes feasible on fractured reservoirs modeled using dual medium flow behavior.

The selection approach aims at representing uncertainty through distances between models, in this case the 156 scenarios. This distance then allows representing high-dimensional models in low-dimensional space using multidimensional scaling (MDS) and allows for grouping scenarios into clusters with similar pattern characteristics. As described earlier in this paper, we have generated four realizations of each scenario leading to 624 patterns. To calculate the distance between the 624 binary patterns, we employ the modified Hausdorff distances (MHD), a distance which has been shown to be effective in distinguishing patterns containing thin lines and sharp objects [40]. A *k*-medoid clustering technique [41, 42] applied in metric space

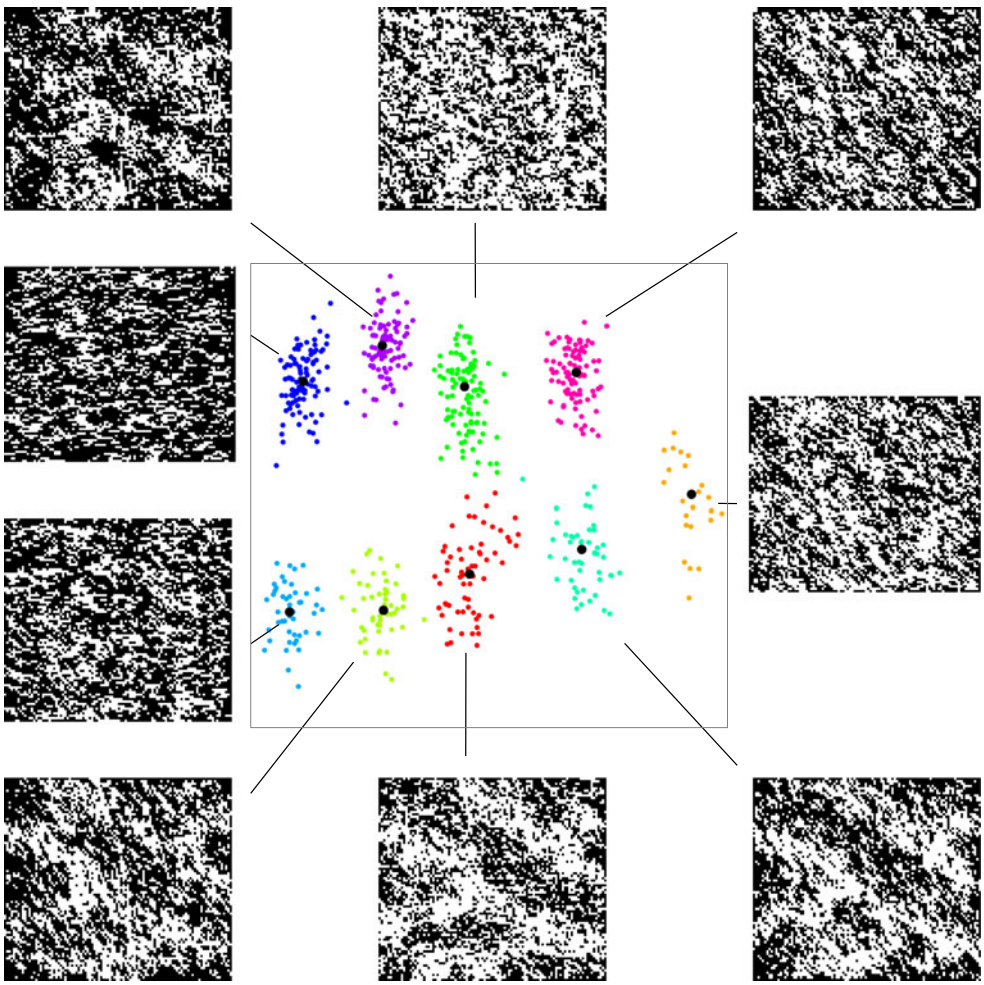

Fig. 6 The modified Hausdorff distance, a pattern-based distance, between the 624 binary maps (4 realizations of 156 scenarios) is mapped into metric space with multidimensional scaling. No absolute scale is shown for location of the data points because only the relative mutual distance is important. Similar patterns are located closer together. Representative patterns are identified with *k*-medoids clustering and will be used as training images

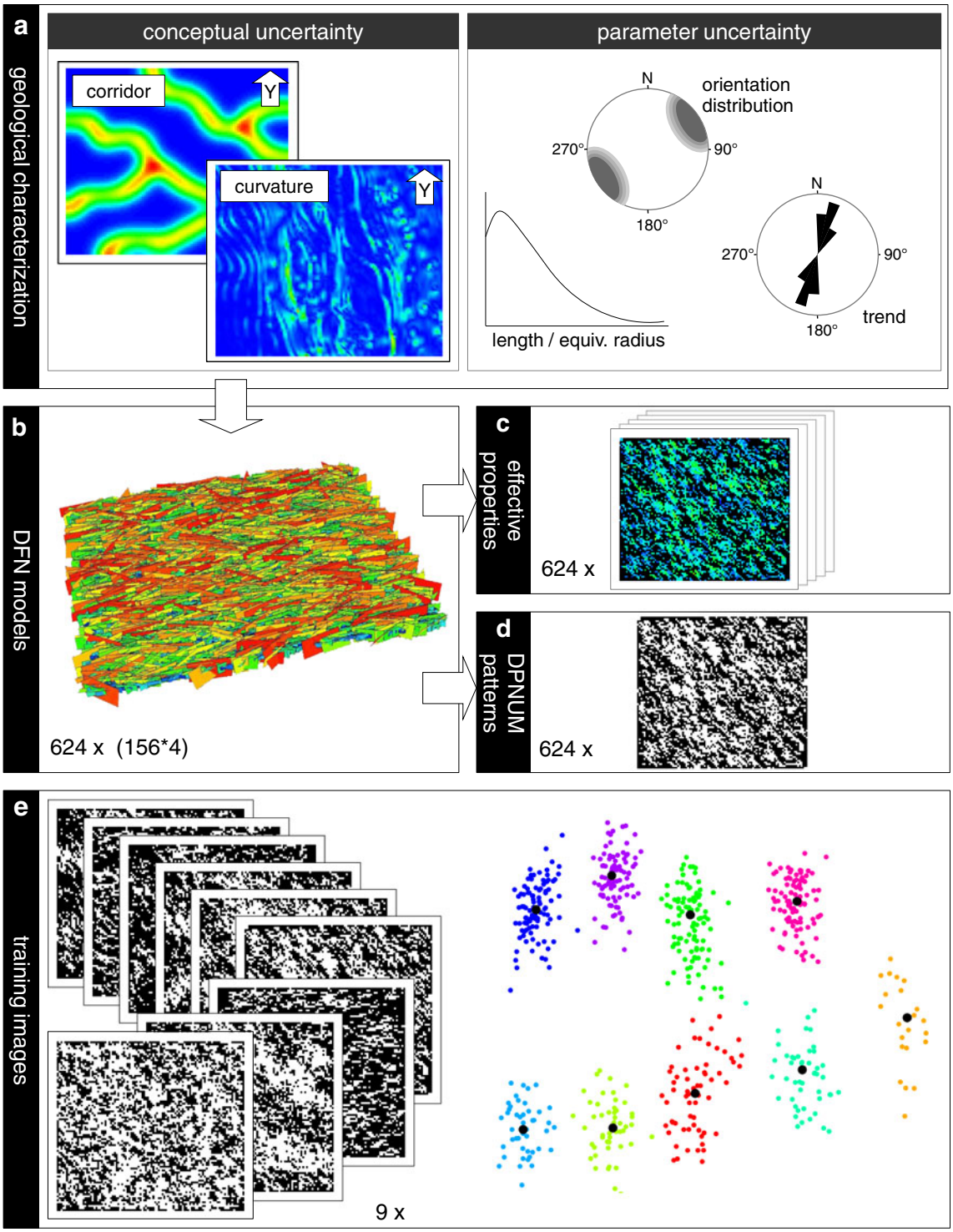

Fig. 7 Overview of the workflow steps take to obtain representative binary DPNUM patterns, i.e., conceptual flow scenarios, as training images without running flow simulation (cf. steps 1–5 in Fig. 1). The conceptual and parameter uncertainty originating from the geological interpretations (**a**) is captured by an experimental design leading to 156 DFN models (**b**). For each DFN, four realizations are generated totaling 624 models. All DFN models are upscaled to effective properties (**c**) and translated to a binary DPNUM map for the flow model (**d**). The binary map determines for which grid cells the fractured medium is considered, i.e., which grid cells are run in dual-porosity mode. **e** K-medoid clustering in metric space is applied to modified Hausdorff distance of the patterns to identify representative training images

then allows the selection of a limited set of representative scenarios. We performed the clustering on the first two dimensions of the Euclidean space created by MDS for which the silhouette technique [43] indicates an optimal number of nine clusters. MHD separates the patterns clearly into well-defined clusters. The patterns corresponding to the nine medoids are then used as training images (Fig. 6) in the following steps of the workflow, and are capable of capturing uncertainty reasonably as shown in Section 3. Note that the use of a MHD distance does not require running any flow simulation; hence, the selection technique is instantaneous. The workflow up to this stage is summarized in Fig. 7.

2.6 Generating fracture flow patterns from training images (step 5)

We used the MPS algorithm *dispat* [44] implemented in SGeMS [45] to generate geostatistical binary patterns for the reservoir based on the nine training images obtained in the previous steps (Fig. 7). This allows modeling the within-scenario spatial uncertainty, where each scenario is represented by a single training image. *Dispat* is a public domain fast pattern-based MPS algorithm allowing the use of non-stationary training images [46] (https://github.com/SCRFpublic/DisPat). A comparison of the patterns obtained from initial DFN models and patterns generated with MPS is shown in Fig. 8. Once the basic flow model represented through the binary map is generated, the dual medium cells (shown in white) are populated with appropriate effective properties for the fractured medium. For simplification, we populate the fractured medium with the constant average of each property, although this is not a restriction to the methodology. How this is done specifically for this case as well as the impact on the flow response is discussed in Section 3, since this is not part of the intended original contribution of this paper.

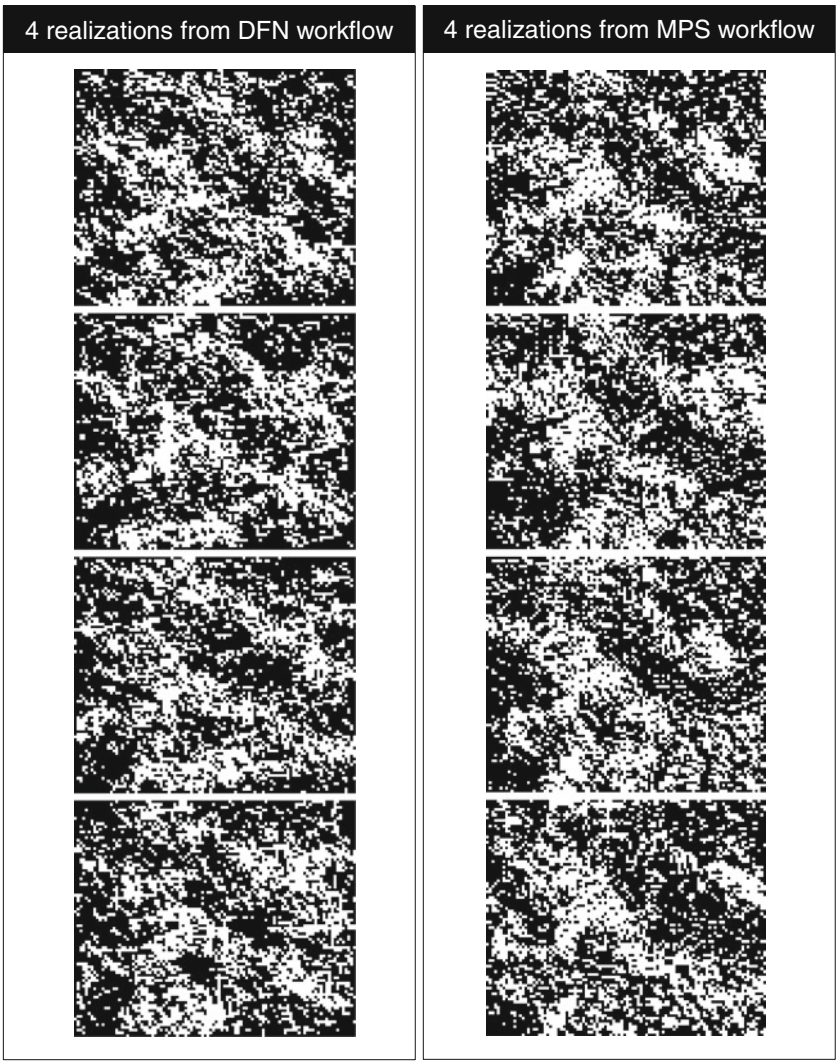

Fig. 8 Comparison of binary DPNUM patterns obtained from DFN workflow (cf. steps 1–3 of the proposed workflow) and from the MPS workflow (cf. steps 6–7 of the proposed workflow). While it took several minutes to generate one pattern with the DFN workflow, it took only 50 ms to simulate one pattern with the MPS algorithm *dispat*

3 Results

The goal of this study is to assess rapidly the field production performance of a large number of models. The clustering of patterns based on the MHD was performed on the entire reservoir scale; hence, the selected nine patterns are targeted to predict global field production, not individual well performance. In this section, we will first assess which factor has the largest impact on field production: dual medium properties (DPNUM) versus effective properties ($k_f, \emptyset_f, \sigma$). Secondly, we will compare the range of uncertainty, i.e., the variability, in flow responses between two workflows to which we refer for convenience as "DFN workflow" and "MPS workflow". The DFN workflow consists of generating DFN models, upscaling the fractures to effective properties, and running flow simulations on the dual medium models. This would be the more standard approach. In the MPS workflow, the dual medium models are directly generated with MPS (step 5 of the workflow proposed in this paper) based on the selected training images obtained in step 4, and then flow simulated as well. This comparison will therefore assess the effectiveness of the proposed workflow.

3.1 Impact of dual medium pattern versus effective properties

Our contribution focusses on dual medium patterns (DPNUM) and spatial distribution. However, flow simulation also requires specifying effective medium properties, such as porosity and permeability for both dual and single medium cells, as well as the shape factor (σ). Since the patterns generated with MPS are variations of the patterns in the training image, it is not possible to simply copy the effective properties associated with each training image. To populate the dual medium cells of MPS-simulated patterns rapidly with reasonable effective properties for the fractured medium, we have decided to use the constant average of each property (Fig. 9). The average is calculated for each fracture property (k_f, ϕ_f, σ) associated with the training image individually while only considering dual medium cells. As we will show in this section, using a constant average does not impact the flow response in our case because the dual medium pattern is the most impacting factor. In the following, we will compare different ways to populate the dual medium cells with effective properties only focusing on the fractured medium because in our case, the single medium cells contain only the properties of the matrix which are fixed and constant. To evaluate the impact of the dual medium pattern versus the effective properties, we populated the fractured medium of dual medium cells

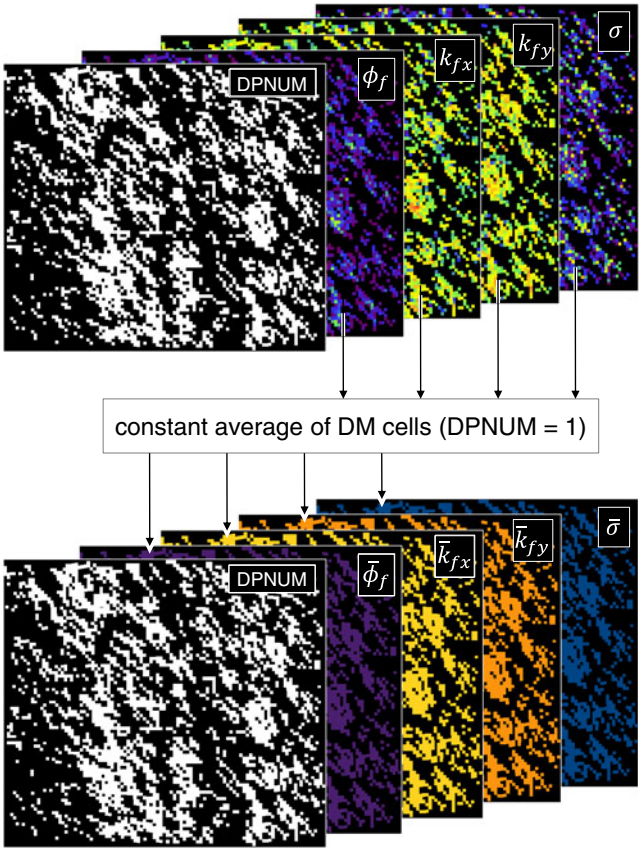

Fig. 9 Calculation of the constant average for each property of the fractured medium and sigma. Only dual medium cells as indicated by DPNUM are considered. The constant average is used to populate the fractured medium of DPNUM patterns simulated with *dispat* (MPS). In this particular example, the same DPNUM pattern is populated with effective properties (cf. path 2 in flow diagram of Fig. 10)

of two dual medium patterns in three different fashions (see diagram in Fig. 10):

1. Copy original properties associated with the dual medium pattern
2. Calculate the constant average for each original property
3. Multiply/divide the constant average of each property by a factor of 10 through a 3^4 full factorial design (Table 2).

To be able to compare (2) and (3) with the flow responses resulting from the original properties, we have used two patterns from the 624 patterns obtained from the DFN workflow. The flow responses shown in Fig. 10 show a clear separation of the curves into two groups related to the two different patterns. It can also be observed that the flow responses based on the constant average (2) properties run very close and mostly overlay with the curves obtained by using the original properties (1). The curves of

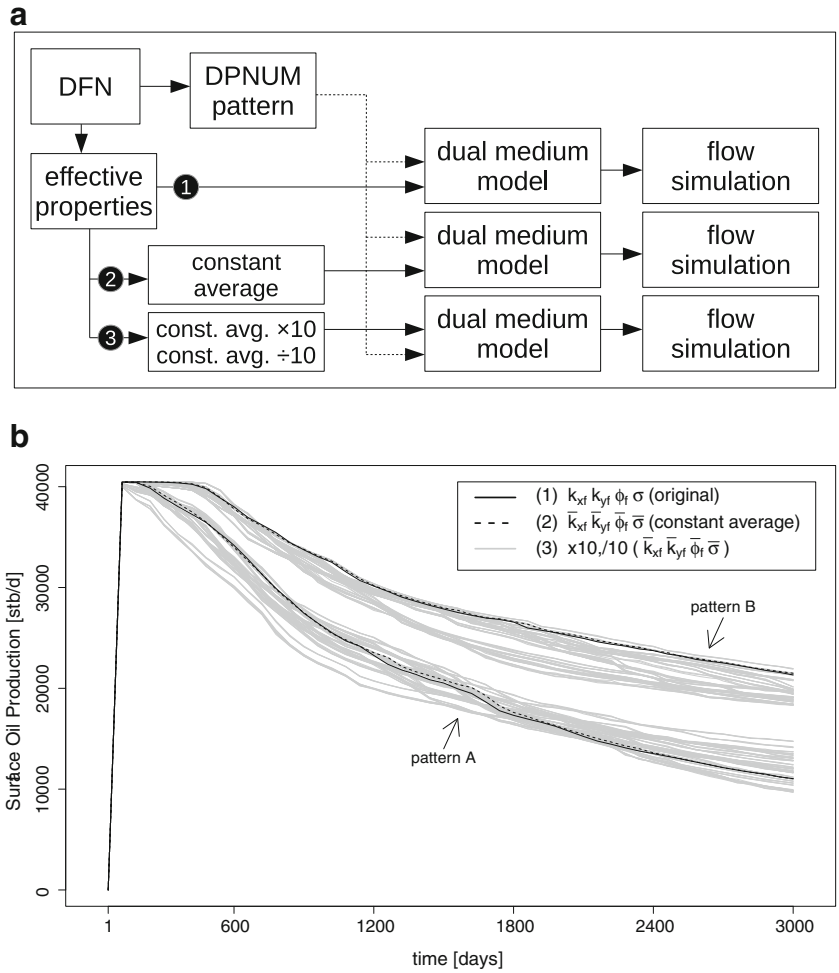

Fig. 10 Impact of dual medium properties (DPNUM) versus effective properties. Two different patterns (produced from two different DFNs) and three different ways of obtaining the effective properties are compared. The flow diagram shows three fashions of populating the fractured medium of one dual medium pattern (DPNUM). The same steps are applied to both DFNs. First, a DFN model is translated to a dual medium pattern (DPNUM) and upscaled to effective properties. Besides the original effective properties from upscaling (path 1) the same pattern is also populated in two different fashions with effective properties. Path 2: constant average for each property based on the original ones (cf. Fig. 9). Path 3: the averages are multiplied and divided by factor 10, respectively. The comparison of the flow responses shows in our case that the binary dual medium patterns (DPNUM) strongly govern the flow response, whereas the way of populating the dual medium cells has only a minor impact: flow responses based on the original and averaged effective properties run very close. Even flow responses based on heavily varied (factor 10) properties can be clearly associated with their corresponding pattern

the flow responses based on heavy variation of the effective properties (3) diverge from the flow responses based on the original (1) and averaged (2) properties. However, the differentiation of the flow responses into two distinct groups is caused by the two patterns. Clearly, the pattern of dual medium cells is the dominating factor.

Table 2 Full factorial experimental design leads to 81 combinations of effective property variations per pattern

k_{fx}	Const. avg.	×10	÷10
k_{fy}	Const. avg.	×10	÷10
ϕ_f	Const. avg.	×10	÷10
σ	Const. avg.	×10	÷10

3.2 Comparison of range of uncertainty

In this section, we will show that our proposed MPS workflow is suitable to fully cover the uncertainty in flow response in a fraction of the time required by the DFN workflow. Therefore, we will evaluate and compare flow responses of reservoir models generated by the two workflows (see flow diagram in upper half of Fig. 11). For the

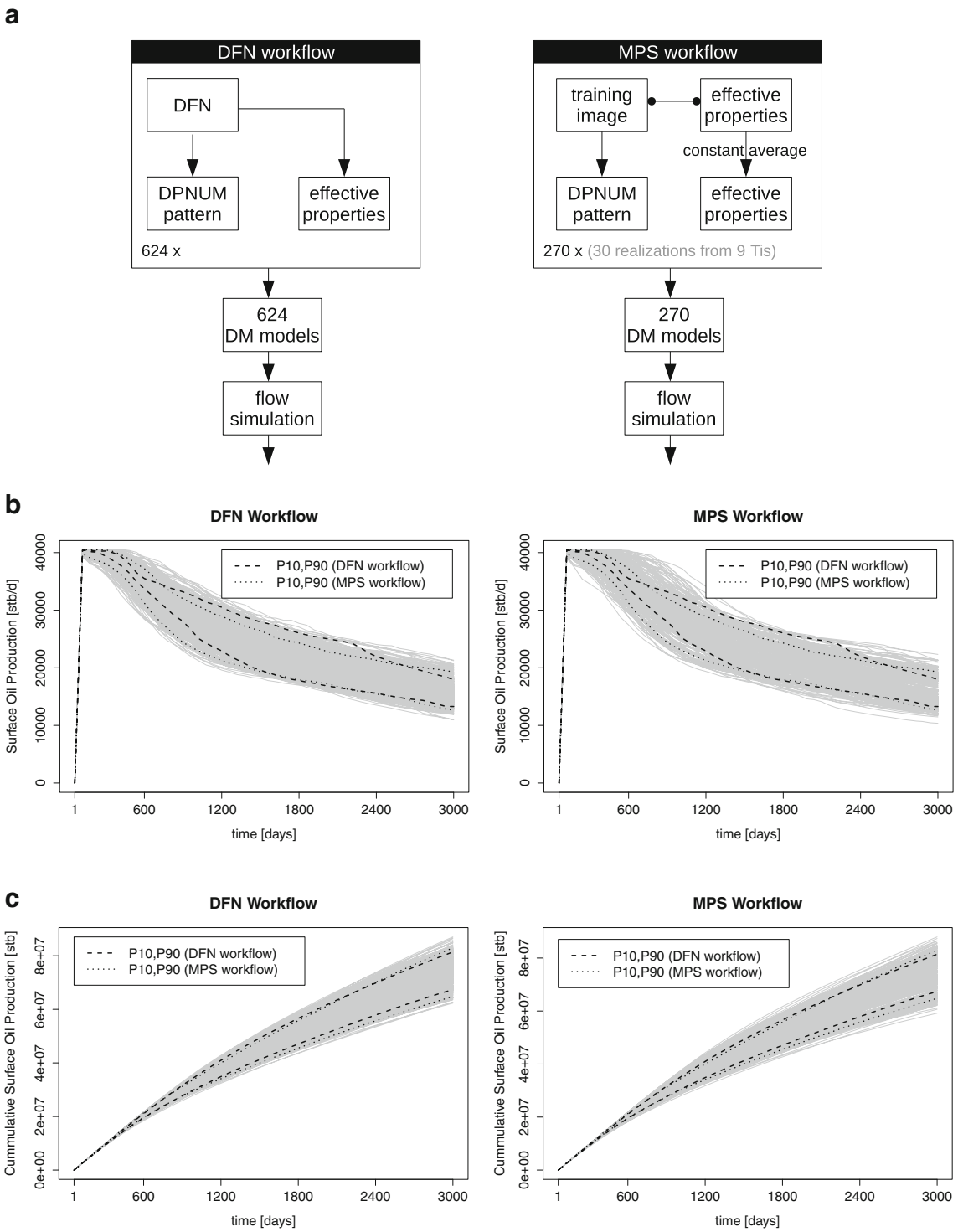

Fig. 11 Comparison of uncertainty in the flow responses for fractured reservoirs obtained from the proposed training images based MPS workflow with the DFN-based workflow. Flow was simulated for 624 dual media model originating from DFN models, and for 270 dual media models generated with the MPS workflow. P10 and P90 of both workflows are shown in both plots to facilitate comparison. P10 and P90 of the MPS-based workflow describe at least the same range of uncertainty as the DFN workflow for fractured reservoirs

DFN workflow, we simulated the flow responses of the 624 reservoir dual medium models created in steps 1–4. These dual medium flow models are obtained through the upscaling of the actual DFN models. The process of DFN generation and upscaling to effective properties took half a minute per model. The time to generate the 624 models was

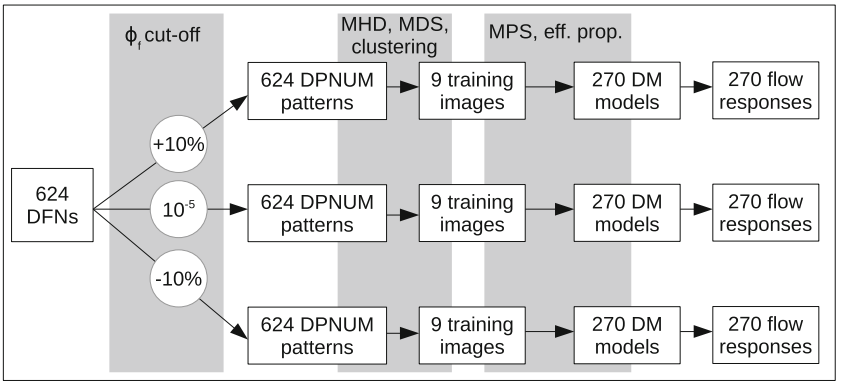

Fig. 12 To compare the impact of the threshold/cutoff on fracture porosity used during the pattern production in step 3 of the workflow, we rerun the workflow for two additional thresholds by increasing and decreasing the original threshold by 10 %

6 h. For the MPS workflow, we simulated the flow response for 270 dual medium models in the following way: based on the nine training images identified in step 5, we generated 30 realizations with the MPS algorithm *dispat*. The variance in flow response from these 30 models originates from the differences in the reproduced binary patterns. The creation of one binary pattern with *dispat* took between 50 and 100 ms; the subsequent population with effective properties is essentially instantaneous. The time to generate the 270 DPNUM patterns was 20 s. Populating the cells of all models with effective fracture properties via the averaging method took 30 s. For the total time, we are looking at 1 min of the MPS workflow versus 1 day for the DFN workflow. Note that the MPS workflow initially depends on the DFN workflow for the creation of training images. In practice, however, the creation of the training image via the DFN workflow is an initial investment which allows later to generate thousands of earth models with the MPS workflow independently and rapidly.

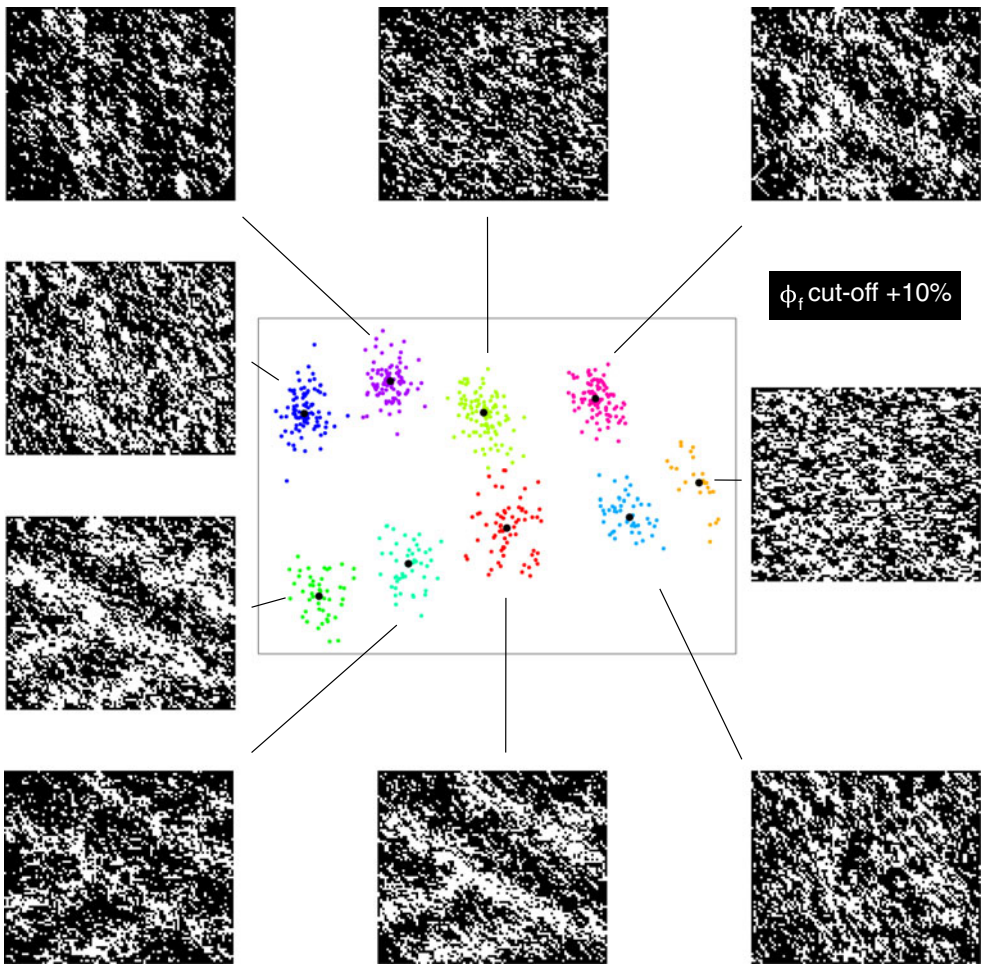

Fig. 13 Training images identified among 624 DPNUM patterns based on a 10 % increased threshold on fracture porosity. The increase of the threshold leads to more delicate patterns

We will now compare the flow responses of the 624 flow models obtained from the DFN workflow with the 270 flow responses from the MPS workflow. The uncertainty quantification is based on the quantiles P10 and P90. The lower part of Fig. 11 shows the flow responses from both workflows. On the left side are the 624 flow responses from the DFN workflow, and on the right side are the 270 flow responses from the MPS workflow. The quantiles P10 and P90 of both workflows are shown in the left and the right side of Fig. 11 to facilitate comparison. The resulting flow responses show that the uncertainty in flow responses obtained from the flow models generated with the MPS-based workflow capture uncertainty reasonably. The curves for P10 and P90 run very close. In this reservoir study, the range of uncertainty covered by the MPS workflow is slightly greater.

3.3 Impact of threshold on patterns and captured uncertainty

In this section, we will evaluate the impact of the cut-off applied to the fracture porosity ($\emptyset_f$) when creating the binary dual medium models (DPNUM) in step 3 of the DFN workflow. Increasing or lowering the cutoff will lead to less or more dual medium cells, and change the appearance of the patterns. Increasing the threshold lowers the number of dual medium cells and leads to more refined patterns. Lowering the threshold increases the number of dual medium cells and leads to more coarse patterns. To evaluate the sensitivity to the fracture porosity threshold, we have increased and lowered the threshold by 10 % in step 3 of the DFN workflow. Changing the threshold by 10 % switches on average also 10 % of the grid cells from single to dual medium and vice versa (Fig. 3). For the upper as well as for the lower threshold, we have applied the complete workflow. The steps taken are summarized in Fig. 12. In short, starting from the original 624 DFN models, we produced two additional sets of 624 binary patterns each corresponding to the two threshold variations (+10 %, −10 %), calculated the modified Hausdorff distance between each group of 624 patterns separately, executed multidimensional scaling (MDS) and k-medoid clustering to identify training images in each group, generated 30 realizations for each training image

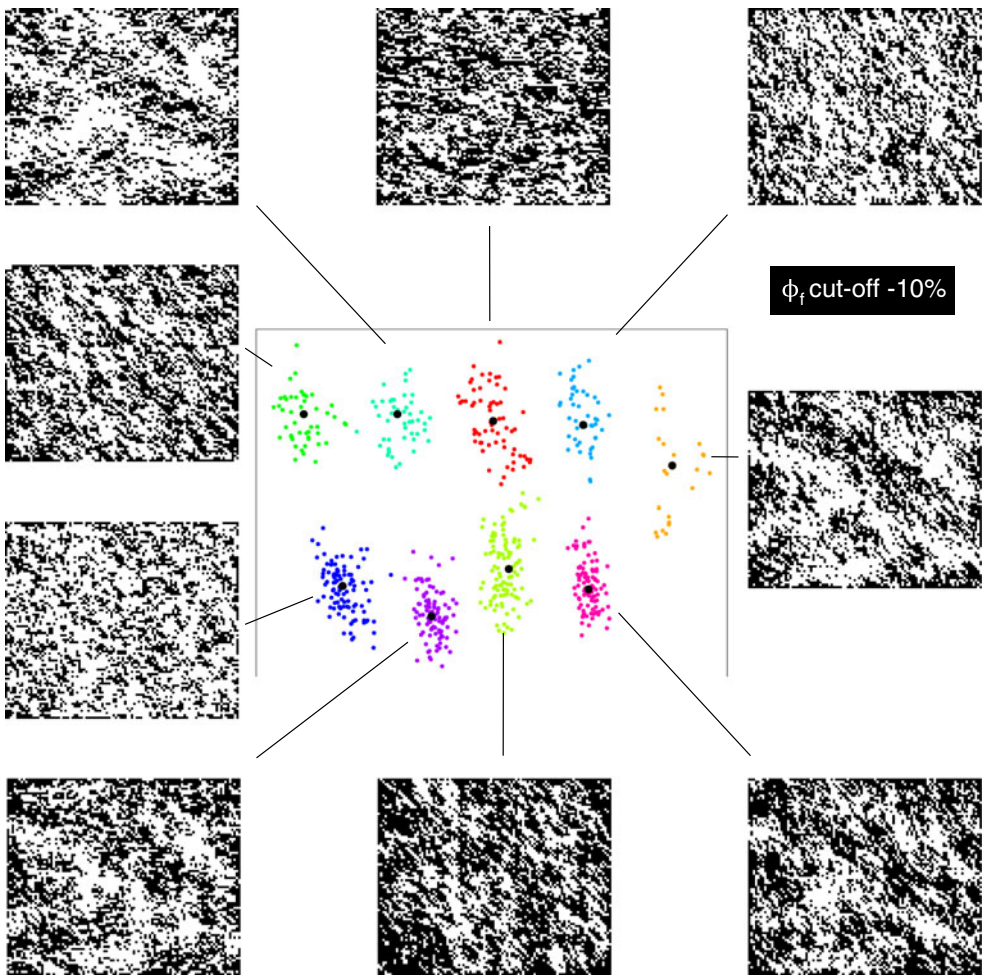

Fig. 14 Training images identified among 624 DPNUM patterns based on a 10 % decreased threshold on fracture porosity. The decrease of the threshold leads to coarser patterns

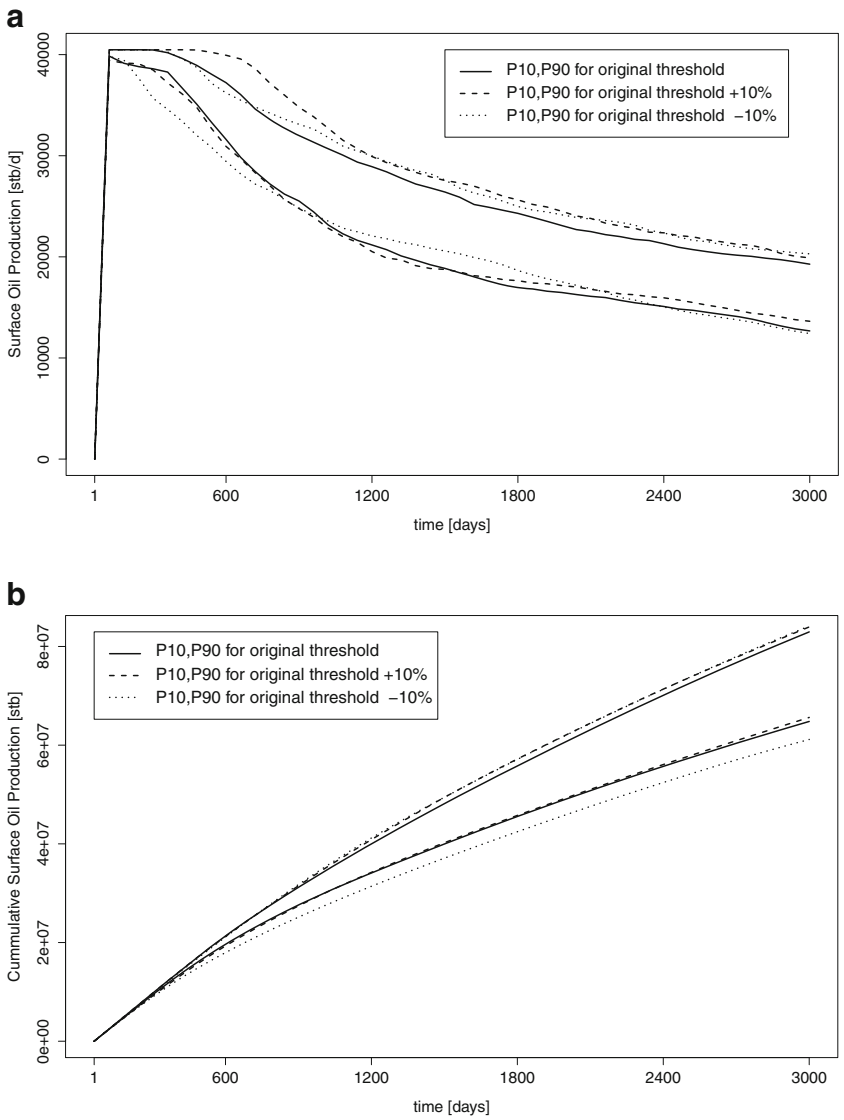

Fig. 15 Evaluation of the impact of the threshold used for DPNUM pattern production on the uncertainty in flow responses. For each of the three different thresholds, the MPS workflow was run and dual medium models were generated for flow simulation. The training images employed are shown in Figs. 6, 13, and 14. In our case the variation of the threshold by 10 % does not influence the range of uncertainty

with *dispat* (MPS), populated the dual medium cells with effective properties, and performed flow simulations. For a detailed explanation of the workflow, please refer to Section 2 of this paper. In the group with 10 % increased threshold, we have identified nine training images shown in Fig. 13. For the 10 % decreased threshold, we also have identified nine training images show in Fig. 14. Although the patterns become either more refined or coarse in comparison to the patterns obtained using the original threshold, the basic structure does not change. All three levels of the threshold lead to nine training images. Figure 15 compares the range of uncertainty (P10, P90) calculated from the flow responses based on three different fracture porosity thresholds (270 flow responses per threshold): original (10^{-5}), +10 %, −10 %. The P10 and P90 for each threshold run very close and capture similar ranges of uncertainty.

4 Conclusions

In this paper, we have introduced a pattern and training image-based approach to dual-porosity descriptions of naturally fractured reservoirs. The patterns of effective properties are obtained from DFN to preserve geologic consistency. Once relevant patterns are obtained, the tedious task of DFN modeling is no longer required. The generation of large numbers of earth models with MPS can be achieved in a fraction of the time and with far fewer computer resources necessary to generate the same amount of DFN models. We have shown that the pattern-based approach is able to capture uncertainty of the flow responses reasonably. Due to the selection of already available components, the proposed workflow will be easy to integrate into existing reservoir modeling software. Further, the modular design of the workflow provides the freedom to employ different

techniques, e.g., for clustering, MPS algorithm, and flow simulations.

Acknowledgments We would like to thank Golder Associates for providing us with the DFN modeling package Fracman, and Streamsim Technologies for the use of 3DSL and studioSL. Also, we would like to thank all sponsors of the Stanford Center for Reservoir Forecasting for supporting our research. We are grateful for the very helpful and constructive comments of our two anonymous reviewers, which helped us to improve this paper.

References

1. Warren, J.E., Root, P.J.: The behavior of naturally fractured reservoirs. Soc. Petr. Eng. J. **3**(3), 245–255 (1963). doi:10.2118/426-PA
2. Dershowitz, B., LaPointe, P., Eiben, T., Wei, L.: Integration of discrete feature network methods with conventional simulator approaches. SPE. Reserv. Eval. Eng. **3**(2), 165–170 (2000). doi:10.2118/62498-PA
3. Cacas, M.C., Daniel, J.M., Letouzey, J.: Nested geological modelling of naturally fractured reservoirs. Pet. Geosci. **7**, 43–52 (2001)
4. Zhong, J., Aydina, A., McGuinness, D.L.: Ontology of fractures. J. Struct. Geol. **31**, 251–259 (2009)
5. Guerriero, V., Iannace, A., Mazzoli, S., Parente, M., Vitale, S., Giorgioni, M.: Quantifying uncertainties in multi-scale studies of fractured reservoir analogues: implemented statistical analysis of scan line data from carbonate rocks. J. Struct. Geol. **32**, 1271–1278 (2010)
6. Caers, J., Zhang, T.: Multiple-point geostatistics: a quantitative vehicle for integrating geologic analogs into multiple reservoir models. In: Grammer, G.M., Harris, P.M., Eberli, G.P. (eds.) Integration of Outcrop and Modern Analogs in Reservoir Modeling, pp. 383–394. AAPG, Tulsa (2002)
7. Strebelle, S.: Conditional simulation of complex geological structures using multiple-point statistics. Math. Geol. **34**, 1–21 (2002)
8. Caers, J., Strebelle, S., Payrazyan, K.: Stochastic integration of seismic data and geologic scenarios: a West Africa submarine channel saga. Lead. Edge **22**, 192–196 (2003)
9. Hu, L.Y., Chugunova, T.: Multiple-point geostatistics for modeling subsurface heterogeneity: a comprehensive review. Water Resour. Res. **44**, W11413 (2008)
10. Daly, C., Caers, J.: Multi-point geostatistics—an introductory overview. First Break **28**, 39–47 (2010)
11. Bond, C.E., Gibbs, A.D., Shipton, Z.K., Jones, S.: What do you think this is? Conceptual uncertainty in geoscience interpretation. GSA Today **17**, 4–10 (2007)
12. Cherpeau, N., Caumon, G., Caers, J., Lévy, B.: Method for stochastic inverse modeling of fault geometry and connectivity using flow data. Math. Geosci. **44**, 147–168 (2012)
13. Feyen, L., Caers, J.: Quantifying geological uncertainty for flow and transport modeling in multi-modal heterogeneous formations. Adv. Water Resour. **29**, 912–929 (2006)
14. Suzuki, S., Caumon, G., Caers, J.: Dynamic data integration for structural modeling: model screening approach using a distance-based model parameterization. Comput. Geosci. **12**, 105–119 (2008)
15. Scheidt, C., Caers, J.: Uncertainty quantification in reservoir performance using distances and Kernel methods—application to a West Africa deepwater turbidite reservoir. SPEJ **14**(4), 680–692 (2009). doi:10.2118/118740-PA
16. Park, H., Scheidt, C., Fenwick, D., Boucher, A., Caers, J.: History matching and uncertainty quantification of facies models with multiple geological interpretations. Comput. Geosci. **17**(4), 609–621 (2013). doi:10.1007/s10596-013-9343-5
17. Bourbiaux, B., Basquet, R., Cacas, M.-C., Daniel, J.-M., Sarda, S.: An integrated workflow to account for multi-scale fractures in reservoir simulation models: implementation and benefits. In: Proceedings of Abu Dhabi International Petroleum Exhibition and Conference (2002)
18. Souche, L., Astratti, D., Aarre, V., Clerc, N., Clark, A., Al Dayyni, T.N.A., Mahmoud, S.L.: A dual representation of multiscale fracture network modelling: application to a giant UAE carbonate field. First Break **30**, 43–52 (2012)
19. Saleri, N.G., Al-Kaabi, A.O., Muallem, A.S.: Haradh III: a milestone for smart fields. J. Pet. Technol. **58**, 28–32 (2006)
20. Streamsim Technologies: 3DSL user manual V 4.10., San Francisco (2013)
21. Ehrenberg, S.N., Nadeau, P.H., Aqrawi, A.A.M.: A comparison of Khuff and Arab reservoir potential throughout the Middle East. AAPG Bull. **91**, 275–286 (2007)
22. Kazemi, H., Merrill, L.S., Porterfield, K.L., Zeman, P.R.: Numerical simulation of water-oil flow in naturally fractured reservoirs. SPE J. **16**(6), 317–326 (1976). doi:10.2118/5719-PA
23. Nelson, R. Geologic Analysis of Naturally Fractured Reservoirs, 2nd edn. Gulf Professional Publishing, Oxford (2001)
24. Zahm, C.K., Hennings, P.H.: Complex fracture development related to stratigraphic architecture: challenges for structural deformation prediction, Tensleep Sandstone at the Alcova anticline, Wyoming. AAPG Bull. **93**, 1427–1446 (2009)
25. Chopra, S., Marfurt, K.J.: Volumetric curvature attributes for fault/fracture characterization. First Break **25**, 35–46 (2007)
26. Narr, W., Schechter, D.S., Thompson, L.B.: Naturally Fractured Reservoir Characterization. Society of Petroleum Engineers, Richardson (2006)
27. Chopra, S.: Coherence cube and beyond. First Break **20**, 27–33 (2002)
28. Neves, F.A., Zahrani, M.S., Bremkamp, S.W.: Detection of potential fractures and small faults using seismic attributes. Lead. Edge **23**, 903–906 (2004)
29. Gabrielsen, R.H.: Characterization of joints and faults. In: Rock Joints: Proceedings of a Regional Conference of the International Society for Rock Mechanics, Loen, 4-6 June 1990, pp. 11–17. Taylor & Francis (Balkema), Rotterdam (1990)
30. Questiaux, J.-M., Couples, G.D., Ruby, N.: Fractured reservoirs with fracture corridors. Geophys. Prospect. **58**, 279–295 (2010)
31. Dershowitz, W.S., Herda, H.H.: Interpretation of fracture spacing and intensity. In: Tillerson and Wawersik (eds.) The 33rd U.S. Symposium on Rock Mechanics (USRMS), June 3–5, 1992, pp. 757–766. American Rock Mechanics Association, Santa Fe, NM, Alexandria (1992)
32. Golder Associates: FracMan 7.4., Redmond (2012)
33. Jones, M.A., Pringle, A.B., Fulton, I.M., O'Neill, S.: Discrete fracture network modelling applied to groundwater resource exploitation in southwest Ireland. Geol. Soc. Lond. Spec. **155**, 83–103 (1999)
34. Snow, D.T.: Anisotropie permeability of fractured media. Water Resour. Res. **5**, 1273–1289 (1969)
35. Brown, S.R.: Fluid flow through rock joints: the effect of surface roughness. J. Geophys. Res.: Solid Earth. **92**, 1337–1347 (1987)
36. Renshaw, C.E., Park, J.C.: Effect of mechanical interactions on the scaling of fracture length and aperture. Nature **386**, 482–484 (1997)
37. Oda, M.: Permeability tensor for discontinuous rock masses. Geotechnique **35**, 483–495 (1985)
38. Caers, J.: Modeling Uncertainty in the Earth Sciences. Wiley, Oxford (2011)

39. Scheidt, C., Caers, J.: Representing spatial uncertainty using distances and kernels. Math. Geosci. **41**, 397–419 (2008)
40. Dubuisson, M.-P., Jain, A.K.: A modified Hausdorff distance for object matching. In: Proceedings of the 12th IAPR International Conference on Pattern Recognition, 1994. Conference A: Computer Vision Image Processing, vol. 1, pp. 566–568 (1994)
41. Maechler, M., Rousseeuw, P., Struyf, A., Hubert, M., Hornik, K.: Cluster: Cluster Analysis Basics and Extensions. R package version 1.14.1 (2011)
42. R Development Core Team: R: A language and environment for statistical computing. R Foundation for Statistical Computing, Vienna (2011)
43. Rousseeuw, P.J.: Silhouettes: a graphical aid to the interpretation and validation of cluster analysis. J. Comput. Appl. Math. **20**, 53–65 (1987)
44. Honarkhah, M., Caers, J.: Stochastic simulation of patterns using distance-based pattern modeling. Math. Geosci. **42**, 487–517 (2010)
45. Remy, N., Boucher, A., Wu, J.: Applied Geostatistics with SGeMS: A User's Guide. Cambridge University Press, Cambridge (2009)
46. Honarkhah, M., Caers, J.: Direct pattern-based simulation of non-stationary geostatistical models. Math. Geosci. **44**, 651–672 (2012)
47. Lees, J.M.: RFOC: Graphics for Spherical Distributions and Earthquake Focal Mechanisms. R package version **3**, 2 (2012)